PRAMANA
— journal of
physics

Vol. 71, No. 1
July 2008
pp. 99–115

Analysis of small-signal intensity modulation of semiconductor lasers taking account of gain suppression

MOUSTAFA AHMED[1,*] and ALI EL-LAFI[2]
[1]Department of Physics, Faculty of Science, Minia University, 61519 El-Minia, Egypt
[2]Department of Physics, School of Basic Science, Academy of Graduate Studies, Tripoli, Libya
[*]Corresponding author. E-mail: moustafafarghal@yahoo.com

MS received 31 August 2007; revised 6 December 2007; accepted 27 December 2007

Abstract. This paper demonstrates theoretical characterization of intensity modulation of semiconductor lasers (SL's). The study is based on a small-signal model to solve the laser rate equations taking into account suppression of optical gain. Analytical forms of the small-signal modulation response and modulation bandwidth are derived. Influences of the bias current, modulation index and modulation frequency as well as gain suppression on modulation characteristics are examined. Computer simulation of the model is applied to 1.55-μm InGaAsP lasers. The results show that when the SL is biased far-above threshold, the increase of gain suppression increases both the modulation response and its peak frequency. The modulation bandwidth also increases but the laser damping rate decreases. Quantitative description of the relationships of both modulation bandwidth vs. relaxation frequency and maximum modulation bandwidth vs. nonlinear gain coefficient are presented.

Keywords. Semiconductor laser; small-signal modulation; modulation response; gain suppression.

PACS Nos 42.55.Px; 42.60.Fc; 42.30.Lr

1. Introduction

A typical advantage of SL's is the fact that they can be directly modulated converting a current signal with a frequency reaching tens of GHz into an optical form [1]. Therefore, the same current is used for both biasing the SL and modulation, which greatly simplifies the external circuitry compared to an external modulator in which several currents are needed [2]. Small-signal sinusoidal modulation at GHz rates has potential applications in reducing the modal noise in optical fiber systems [3] as well as the external optical feedback noise in optical-disc systems [4]. Under strong modulation, one can readily obtain optical pulses as short as a few picoseconds [5], which may be used for time-resolved dynamical studies and for carrying high-bit information in optical communication systems [6].

Typical characteristics of laser modulation can be gained by determining the SL response to small-signal modulation, which measures the amplitude of the modulated signal relative to that of the unmodulated signal [7]. This response looks like a second-order low-pass filter, peaking around the relaxation frequency of the SL [7]. Exploring the small-signal modulation characteristics has been the subject of intensive experimental and theoretical studies [8–17]. It has been seen that the modulation bandwidth is determined by the relaxation frequency and damping rate of laser oscillation, and increases with the bias current up to an upper limit. This ultimate maximum modulation frequency is a direct measure of the maximum speed or bit rate at which information can be transmitted by the laser [2]. Measured values around 20 GHz were reported to the upper modulation frequency of Fabry–Perot (FP) InGaAsP lasers [10]. Several studies were reported to investigate the laser parameters that can push this maximum modulation frequency to higher values [8–13]. The nonlinear property of optical gain and electrical parasitic effects are the cause of the damping effect that limits the maximum modulation frequency [7,10–13,16]. Increasing the differential gain and operating the SL at low temperatures can grow the maximum modulation frequency [7,9,15].

The static and dynamic behaviours of SL's are described by a set of rate equations that describe the temporal evolutions of the photon number, optical phase and injected electron number [18]. The direct analog modulation is taken into account by augmenting an AC component to the current term in the rate equation of the electron number. Due to the coupling and nonlinearity of the rate equations, analytical solutions of the rate equations can be achieved by applying appropriate approximations. This is commonly brought about by the small-signal analysis in which the solutions are given in the frequency domain assuming small changes in the photon and electron numbers compared to their mean components. The small-signal analysis was first applied to the SL theory by Haug [19]. It helps to obtain a good understanding of how the laser would work at high-speed modulation [20], and to formulate expressions of the modulation response and bandwidth.

Dynamics of SL's are influenced by the nonlinear property of optical gain, which originates from intraband relaxation processes of charge carriers that extend for times as short as 0.1 ps [21]. It manifests as suppression of gain just under the threshold gain level when the current increases beyond the threshold value [21]. Although nonlinear gain was proved to influence the modulation bandwidth [7,11,16], quantitative description of the influence of gain suppression on the maximum modulation frequency has been lacked.

This paper demonstrates application of the small-signal analysis to characterize the analog intensity modulation of SL'S. We aim to examine influences of the modulation parameters, namely, bias current, modulation current and modulation index, as well as gain suppression on the characteristics of analog intensity modulation. In the following section, the theory of small-signal modulation is presented and analytical forms of the small-signal modulation response and modulation bandwidth are derived. In §3, numerical analyses of the model are applied to 1.55-μm InGaAsP lasers as the most representative radiation sources in fiber-optic communications. The obtained results correspond to the operation of both conventional and advanced lasers. Dependences of the modulation characteristics on modulation parameters and gain suppression are examined. The role of the damping rate to

set an upper limit to the modulation frequency is illustrated. When available, the simulated results are compared with experimental results. Finally, the conclusions of this work appear in §4.

2. Theory of small-signal modulation

2.1 *Linearization of rate equations*

The analog modulation of SL's is mathematically described by the following rate equations of the photon number $S(t)$ and injected electron number $N(t)$ [20,22]:

$$\frac{\mathrm{d}S}{\mathrm{d}t} = (G - G_{\mathrm{th}})S + \frac{C}{\tau_r}N, \tag{1}$$

$$\frac{\mathrm{d}N}{\mathrm{d}t} = \frac{1}{e}I(t) - AS - \frac{N}{\tau_{\mathrm{e}}}, \tag{2}$$

where G is the optical gain (s^{-1}), and is defined in the nonlinear form [21]

$$G = A - BS \tag{3}$$

with the coefficients of linear gain A and nonlinear gain (gain suppression) B defined as

$$A = \frac{a\xi}{V}(N - N_{\mathrm{g}}), \tag{4}$$

$$B = \frac{9}{2}\frac{\pi\hbar\nu}{\varepsilon_0 n_{\mathrm{a}}^2 V}\left(\frac{\xi\tau_{\mathrm{in}}}{\hbar}\right)^2 aR_{\mathrm{cv}}^2(N - N_{\mathrm{s}}), \tag{5}$$

where a is the tangential gain, ξ is the confinement factor of the optical field in the active layer whose volume is V and refractive index is n_{a}, N_{g} is the electron number at transparency, N_{s} is the electron number characterizing B, τ_{in} is the intraband relaxation time, ν is the lasing frequency, and R_{cv} is the dipole moment. $\hbar$ is the reduced Planck's constant and ε_0 is the dielectric constant in free space. When the SL is biased above the threshold, the electron number $N(t)$ is clamped just above the threshold number N_{th} [21]. Therefore, B in eq. (5) can be approximated as

$$B = \frac{9}{2}\frac{\pi\hbar\nu}{\varepsilon_0 n_{\mathrm{a}}^2 V}\left(\frac{\xi\tau_{\mathrm{in}}}{\hbar}\right)^2 aR_{\mathrm{cv}}^2(N_{\mathrm{th}} - N_{\mathrm{s}}). \tag{6}$$

The threshold gain G_{th} is given in terms of the material loss κ, power reflectivities R_{f} and R_{b} of the front and back front facets, respectively, and length of the active region L as [21]

$$G_{\mathrm{th}} = \kappa + \frac{1}{2L}\ln\left(\frac{1}{R_{\mathrm{f}}R_{\mathrm{b}}}\right) \approx \frac{a\xi}{V}(N_{\mathrm{th}} - N_{\mathrm{g}}). \tag{7}$$

The last term $CN/\tau_{\rm r}$ in eq. (1) describes the rate of increase of S due to spontaneous emission characterized by the radiative lifetime $\tau_{\rm r}$. C is called the spontaneous emission factor, and determines the fraction of the spontaneous emission transferred into the stimulated emission. Near-above threshold, C may be approximated by [23]

$$C \approx \xi a \tau_{\rm r}/V. \tag{8}$$

In the small-signal analysis, a small sinusoidal perturbation in current $I(t)$ is assumed with modulation circular frequency $\Omega_{\rm m} = 2\pi f_{\rm m}$, where $f_{\rm m}$ is the modulation frequency. That is,

$$I(t) = I_{\rm b} + I_{\rm m}\cos(\Omega_{\rm m} t) = I_{\rm b} + \left(\frac{I_{\rm m}}{2}{\rm e}^{j\Omega_{\rm m} t} + {\rm c.c.}\right) \tag{9}$$

with $I_{\rm m} \ll I_{\rm b}$ and $I_{\rm b} > I_{\rm th}$, and c.c. referring to the complex conjugate term. Both $S(t)$ and $N(t)$ are reasonably supposed to be separated into a DC term and a modulation term as

$$S(t) = S_{\rm b} + \left(\frac{S_{\rm m}}{2}{\rm e}^{j\Omega_{\rm m} t} + {\rm c.c.}\right) \tag{10}$$

$$N(t) = N_{\rm b} + \left(\frac{N_{\rm m}}{2}{\rm e}^{j\Omega_{\rm m} t} + {\rm c.c.}\right) \tag{11}$$

in a similar fashion to the injection current $I(t)$ on the conditions that

$$N_{\rm m} \ll N_{\rm b} \quad \text{and} \quad S_{\rm m} \ll S_{\rm b}.$$

By substituting eqs (9)–(11) into rate equations (1) and (2), separating equations of both bias and modulation terms, employing the small-signal approximation, and neglecting the terms of higher harmonics, we obtain the following pair of equations for the bias components:

$$\{A_{\rm b} - BS_{\rm b} - G_{\rm th}\}S_{\rm b} + \frac{C}{\tau_{\rm r}}N_{\rm b} = 0 \tag{12}$$

$$-A_{\rm b}S_{\rm b} - \frac{N_{\rm b}}{\tau_{\rm e}} + \frac{I_{\rm b}}{\rm e} = 0 \tag{13}$$

and another pair of linear equations for the modulation components

$$-\{\Gamma_{\rm S} + j\Omega_{\rm m}\}S_{\rm m} + \frac{a\xi}{V}\left(S_{\rm b} + \frac{CV}{a\xi\tau_{\rm r}}\right)N_{\rm m} = 0 \tag{14}$$

$$-A_{\rm b}S_{\rm m} - \{\Gamma_{\rm N} + j\Omega_{\rm m}\}N_{\rm m} + \frac{I_{\rm m}}{e} = 0 \tag{15}$$

where $A_{\rm b} = (a\xi/V)(N_{\rm b} - N_{\rm g})$ is the bias component of linear gain A. $\Gamma_{\rm S}$ and $\Gamma_{\rm N}$ are the damping rates of $S(t)$ and $N(t)$, respectively, and are given by

$$\Gamma_{\rm S} = -(G_{\rm b} - G_{\rm th}) + BS_{\rm b} = BS_{\rm b} + \frac{C}{\tau_{\rm r}}\frac{N_{\rm b}}{S_{\rm b}}, \quad \text{using eq. (12)} \tag{16}$$

$$\Gamma_{\rm N} = \frac{a\xi}{V}S_{\rm b} + \frac{1}{\tau_{\rm e}}. \tag{17}$$

Equation (16) indicates that the damping of $S(t)$ originates from both the difference of gain and cavity loss $(G_{\rm b} - G_{\rm th})$ and gain suppression $(BS_{\rm b})$. Near the threshold level, where $B \approx 0$, this damping is determined by the spontaneous emission factor C, whereas far-above threshold, it is governed by gain suppression. Both eqs (16) and (17) indicate that the damping rates of oscillations of $S(t)$ and $N(t)$ increase with the increase of $S_{\rm b}$.

2.2 *Bias components*

The bias component $N_{\rm b}$ of $N(t)$ is determined from eq. (13) as

$$N_{\rm b} = \frac{\frac{a\xi}{V}N_{\rm g}S_{\rm b} + \frac{I_{\rm b}}{e}}{\frac{a\xi}{V}S_{\rm b} + \frac{1}{\tau_{\rm e}}}. \tag{18}$$

The bias component $S_{\rm b}$ of $S(t)$ is then determined as the positive real root of the equation

$$BS_{\rm b}^3 + \left(\frac{BV}{a\xi\tau_{\rm e}} + G_{\rm th}\right)S_{\rm b}^2 - \left(\frac{I_{\rm b}}{e} - \frac{N_{\rm th}}{\tau_{\rm e}} + \frac{C}{\tau_{\rm r}}N_{\rm g}\right)S_{\rm b} - \frac{CV}{a\xi\tau_{\rm r}}\frac{I_{\rm b}}{e} = 0 \tag{19}$$

which can be approximated above threshold in terms of the threshold current $I_{\rm th} = eN_{\rm th}/\tau_{\rm e}$ as

$$S_{\rm b} = (I_{\rm b} - I_{\rm th})/eG_{\rm th}. \tag{20}$$

2.3 *Small-signal modulation response*

The modulation component $N_{\rm m}$ of $N(t)$ is determined from eq. (15) in terms of the corresponding component $S_{\rm m}$ of $S(t)$ as

$$N_{\rm m} = \frac{\Gamma_{\rm S} + j\Omega_{\rm m}}{\frac{a\xi}{V}(S_{\rm b} + \frac{CV}{a\xi\tau_{\rm r}})}S_{\rm m}. \tag{21}$$

The component $S_{\rm m}$ is then determined by substituting for $N_{\rm m}$ in eq. (14).

$$S_{\rm m}(\Omega_{\rm m}) = \frac{\frac{a\xi}{V}\{S_{\rm b} + 1\}}{\Omega_{\rm r}^2 + 2j\Omega_{\rm m}\Gamma_{\rm r} - \Omega_{\rm m}^2}\frac{I_{\rm m}}{e}, \tag{22}$$

where $\Omega_r = 2\pi f_r$ defines the relaxation circular frequency, with f_r being the relaxation frequency, and Γ_r defines the average damping rate of the SL. They are given by

$$\Omega_r^2 = \frac{a\xi}{V}\{S_b + 1\}A_b + \Gamma_N\Gamma_S \tag{23}$$

$$\Gamma_r = \frac{1}{2}(\Gamma_N + \Gamma_S) = \frac{1}{2}\left(\frac{1}{\tau_e} + \frac{a\xi}{V}S_b + BS_b + \frac{C}{\tau_r}\frac{N_b}{S_b}\right). \tag{24}$$

The analog modulation performance of SL's is evaluated in terms of the small-signal modulation response, which defines the transfer function from current modulation to optical power output [7]. At a specific bias current I_b, the modulation response $H_m(\Omega_m)$ at a given modulation frequency Ω_m is defined as the ratio of the modulated photon number $S_m(\Omega_m)$ to the corresponding unmodulated value $S_m(0)$. By using eq. (24), $H_m(\Omega_m)$ is then given by

$$H(\Omega_m) = \frac{S_m(\Omega_m)}{S_m(0)} = \left\{1 + 2j\frac{\Omega_m\Gamma_r}{\Omega_r^2} - \left(\frac{\Omega_m}{\Omega_r}\right)^2\right\}^{-1}. \tag{25}$$

This equation can be written in the form formulated by Petermann [7] as

$$H(\Omega_m) = \left\{1 + j\frac{\Omega_m}{\Omega_d} - \left(\frac{\Omega_m}{\Omega_r}\right)^2\right\}^{-1}, \tag{26}$$

where $\Omega_d = 2\pi f_d = \Omega_r^2/2\Gamma_r$ defines the damping circular frequency of the laser with f_d being the damping frequency.

It is easy to see that in the regime of low-modulation frequencies, $|H(\Omega_m \to 0)| = 1$. The response $|H_m(\Omega_m)|$ exhibits a peak at the modulation frequency

$$\Omega_{m(peak)} = \Omega_r\sqrt{1 - \frac{\Omega_r^2}{2\Omega_d^2}}. \tag{27}$$

The peak value $|H_m|_{peak}$ is obtained by substituting for $\Omega_{m(peak)}$ into eq. (26) giving

$$|H_m|_{peak} = \left\{\frac{\Omega_r}{\Omega_d}\sqrt{1 - \frac{\Omega_r^2}{4\Omega_d^2}}\right\}^{-1}. \tag{28}$$

It is clear that $|H_m|_{peak} = 1$ (flat response) and the peak disappears, $\Omega_{m(peak)} = 0$, when the relaxation frequency Ω_r satisfies

$$\Omega_r = \sqrt{2}\Omega_d. \tag{29}$$

2.4 *Modulation bandwidth*

At a given bias current I_b, the bandwidth of the small-signal modulation response defines the maximum modulation frequency of the SL. This bandwidth is determined as the 3dB frequency $f_{3dB} = \Omega_{-3dB}/2\pi$, or the frequency at which the modulation response $|H_m(\Omega_m)|$ drops to one half of its value $|H(\Omega_m \to 0)|$. Therefore, f_{3dB} is given as

$$\begin{aligned} f_{3dB} &= \frac{\Omega_r}{2\pi}\sqrt{\left(1-\frac{\Omega_r^2}{2\Omega_d^2}\right)+\sqrt{\left(2-\frac{\Omega_r^2}{2\Omega_d^2}\right)^2+\frac{\Omega_r^2}{\Omega_d^2}}} \\ &= \frac{1}{2\pi}\sqrt{(\Omega_r^2-2\Gamma_r^2)+2\sqrt{(\Omega_r^2-\Gamma_r^2)^2+\Omega_r^2\Gamma_r^2}} \end{aligned} \tag{30}$$

which can be approximated following the assumption of Agrawal [11,24] that $\Omega_r \gg \Gamma_r$ as

$$f_{3dB} \approx \sqrt{3}\frac{\Omega_r}{2\pi} = \sqrt{3}f_r. \tag{31}$$

Expression (23) of the relaxation frequency f_r can be simplified to

$$\begin{aligned} f_r^2 &\approx \frac{1}{4\pi^2}\left(\frac{a\xi}{V}\right)\left[\frac{a\xi}{V}(N_b-N_g)\ +BS_b\right]S_b \\ &= \frac{1}{4\pi^2}\left(\frac{a\xi}{V}\right)\left[\frac{a\xi\tau_e}{eV}(I_b-I_g)+B\frac{I_b-I_{th}}{eG_{th}}\right]\frac{I_b-I_{th}}{eG_{th}}, \end{aligned} \tag{32}$$

where $I_g = eN_g/.\tau_e$ is the transparency current. The accuracy of approximation (31) will be examined in the following section of numerical calculations. The above equations show that both f_r and f_{3dB} depend on both the bias current I_b and the nonlinear gain coefficient B.

The bandwidth of the flat modulation response is a critical laser parameter; it defines the upper limit of the modulation frequency. Clearly, this maximum modulation bandwidth $f_{3dB(max)}$ corresponds to $f_r = \sqrt{2}f_d$. Therefore $f_{3dB(max)}$ is determined by the damping frequency f_d (or the damping rate Γ_r) of the SL, i.e., f_d represents a fundamental limit of modulation.

3. Numerical calculations and discussion

In this section, numerical analyses of the small-signal modulation characteristics of SL's are introduced. This is based on numerical calculations of the small-signal modulation expressions derived above. The electron lifetime τ_e in eq. (2) is defined in terms of both the spontaneous emission lifetime τ_r and nonradiative lifetime τ_{nr} as [22]

$$\frac{1}{\tau_e} = \frac{1}{\tau_r} + \frac{1}{\tau_{nr}}. \tag{33}$$

Table 1. Typical values of the parameters of a 1.55-μm InGaAsP laser.

Symbol	Meaning	Value	Unit
λ	Emission wavelength	1.55	μm
a	Tangential gain coefficient	7.85×10^{-12}	$m^3\ s^{-1}$
ξ	Field confinement factor in the active layer	0.2	–
V	Volume of the active region	60	μm^3
L	Length of the active region	250	μm
N_a	Refractive index of the active region	3.56	–
N_g	Electron number at transparency	5.31×10^{7}	–
C	Spontaneous emission factor	2.5×10^{-5}	–
τ_r	Radiative recombination lifetime	7.772	ns
τ_{nr}	Nonradiative recombination lifetime	4.45	ns
τ_{in}	Electron intraband relaxation time	0.1	Ps
$\lvert R_{cv}\rvert^2$	Squared absolute value of the dipole moment	8.575×10^{-57}	$C^2\ m^2$
N_s	Electron number characterizing nonlinear gain	4.05×10^{7}	–
R_f	Reflectivity at the front facet	0.95	–
R_b	Reflectivity at the back facet	0.85	–
κ	Coefficient of material loss	500	m^{-1}

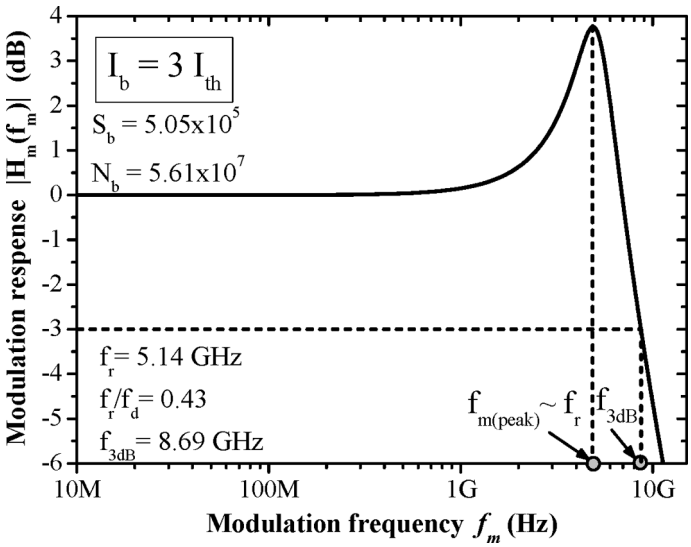

Figure 1. Modulation response $|H_m(f_m)|$ when $I_b = 3I_{th}$. The spectrum exhibits a peak around f_r. The bandwidth is f_{3dB}.

FP-InGaAsP lasers emitting at wavelength $\lambda = 1.55$ μm are considered in the calculations. Typical values of the parameters of these lasers are listed in table 1. The calculated threshold current is 3.17 mA. The calculated nonlinear gain coefficient is set as B_0 and is equal to 683 s^{-1}. Influence of gain suppression on modulation characteristics is examined by varying the coefficient B in eq. (6) relative to the fixed value B_0.

3.1 *Small-signal modulation response*

Figure 1 plots a typical frequency spectrum of the modulation response $|H_{\rm m}(f_{\rm m})|$ when $I_{\rm b} = 3I_{\rm th}$. The figure shows that $|H_{\rm m}(f_{\rm m})|$ exhibits a pronounced peak at a frequency $f_{\rm m(peak)} = 4.9$ GHz close to the relaxation frequency $f_{\rm r} = 5.14$ GHz. In this case, the damping frequency $f_{\rm d}$ is higher than $f_{\rm r}$ ($f_{\rm r} = 0.43 f_{\rm d}$) and the modulation bandwidth $f_{\rm 3dB} = 8.69$ GHz. The spectrum of $|H_{\rm m}(f_{\rm m})|$ can be understood by breaking it into three sections: the plateau, peak, and the declining region [25]. When $f_{\rm m} \ll f_{\rm r}$, the charge carriers can follow the change of the injection current and the laser hardly changes the CW operation, resulting in a flat response. Within the region of peak response, in addition to the response to the change of the injection current, the carriers also interact with the photon field. This is similar to the transient effect observed after the SL is turned on. A complete phase synchronous between the injected electrons and photon field leads to the general laser resonance characterized by $f_{\rm r}$. The next declining part of $|H_{\rm m}(f_{\rm m})|$ is due to the fact that the phase of the photon field lags behind that of the injection current. As $f_{\rm m}$ is increased beyond $f_{\rm m(peak)}$, the electron and photon fields tend to become more and more out of phase, resulting in damping of the relaxation oscillations, and monotonic decrease of $|H_{\rm m}(f_{\rm m})|$.

3.2 *Influence of bias current on modulation characteristics*

Before discussing the influence of bias current on the modulation response, it is beneficial to study its influence on the damping rates $\Gamma_{\rm S}$, $\Gamma_{\rm N}$ and $\Gamma_{\rm r}$ of the laser. The origins of these damping rates from the difference of gain and loss $(G - G_{\rm th})$, or equivalently spontaneous emission, gain suppression and photon number $S_{\rm b}$ are illustrated. Figure 2a plots the variation of $\Gamma_{\rm S}$ with $I_{\rm b}$ and the individual contributions from the terms of spontaneous emission $(C/\tau_{\rm r})(N_{\rm b}/S_{\rm b})$ and gain suppression $BS_{\rm b}$ in eq. (16). The figure shows that $\Gamma_{\rm S}$ is dominated by gain suppression, increasing linearly with $I_{\rm b}$ (i.e. with $S_{\rm b}$). The spontaneous emission has very small values, decreasing rapidly with the increase of $I_{\rm b}$ near $I_{\rm th}$. Therefore, $\Gamma_{\rm S}$ can be approximated by

$$\Gamma_{\rm S} \approx BS_{\rm b} = B\frac{I - I_{\rm th}}{eG_{\rm th}}. \tag{34}$$

The corresponding variations of $\Gamma_{\rm N}$ and the individual contributions from the terms of photon number $a\xi/VS_{\rm b}$ and electron lifetime $1/\tau_{\rm e}$ in eq. (17) are plotted in figure 2b. The figure shows that $\Gamma_{\rm N}$ is dominated by the term $a\xi/S_{\rm b}$ increasing linearly with $I_{\rm b}$ (i.e. with $S_{\rm b}$). Therefore, $\Gamma_{\rm N}$ is effectively approximated by

$$\Gamma_{\rm N} = \frac{a\xi}{V}S_{\rm b} \approx \frac{a\xi}{V}\frac{I - I_{\rm th}}{eG_{\rm th}}. \tag{35}$$

Comparing the numerical ranges of figures 2a and b points out that $\Gamma_{\rm N}$ is much higher than $\Gamma_{\rm S}$ which is opposite to the approximation of Petermann in ref. [7]. This difference stems from two assumptions by Petermann [7]. First, equal rates

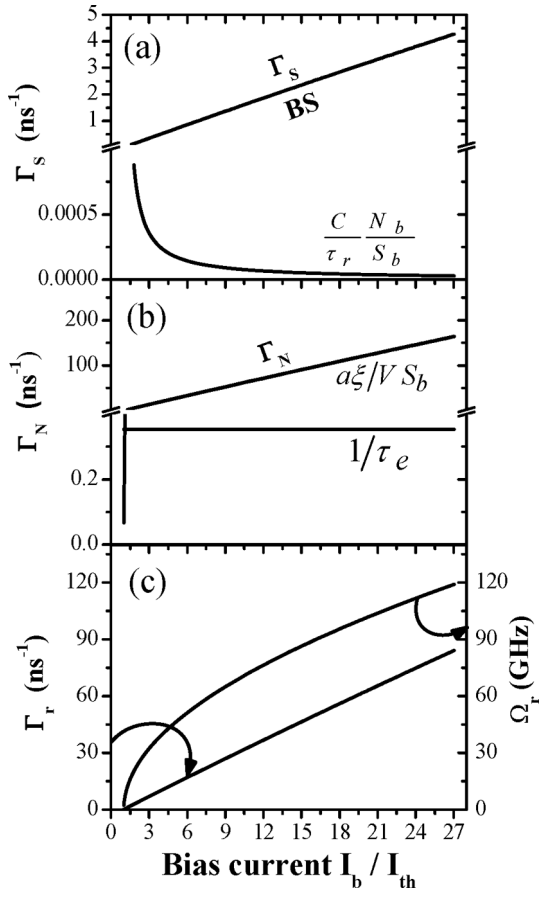

Figure 2. Influence of I_b on damping rates (**a**) Γ_S of $S(t)$, (**b**) Γ_N of $N(t)$ and (**c**) rate Γ_r and the relaxation circular frequency Ω_r.

were assumed for both stimulated and spontaneous emission in rate equation (1) of $S(t)$, which results in the approximation of eq. (8). This approximation would overestimate the spontaneous emission term in eq. (16). On the other hand, Petermann took account of gain suppression in rate equation (2) of $N(t)$, which adds a negative large-valued term of gain suppression to the right-hand side of eq. (17) and decreases Γ_N. The present rate equation model is derived from the density-matrix analysis of nonlinear gain [21], in which the rate of change of the injected electrons $N(t)$ is controlled by linear gain and is not influenced by gain suppression. Equations (34) and (35) indicate that the damping rate Γ_r of the laser increases linearly with S_b and I_b as

$$\Gamma_\mathrm{r} = \frac{1}{2}\left(\frac{a\xi}{V} + B\right) S_\mathrm{b} = \frac{1}{2}\left(\frac{a\xi}{V} + B\right) \frac{I_\mathrm{b} - I_\mathrm{th}}{eG_\mathrm{th}} \tag{36}$$

which is illustrated in figure 2c. The above discussion shows that the laser damping originates from the gain suppression as well as the rapid increase of the photon number S_b above the threshold. Figure 2c plots also on the right-hand axis the corresponding variation of the relaxation circular frequency Ω_r. This figure shows

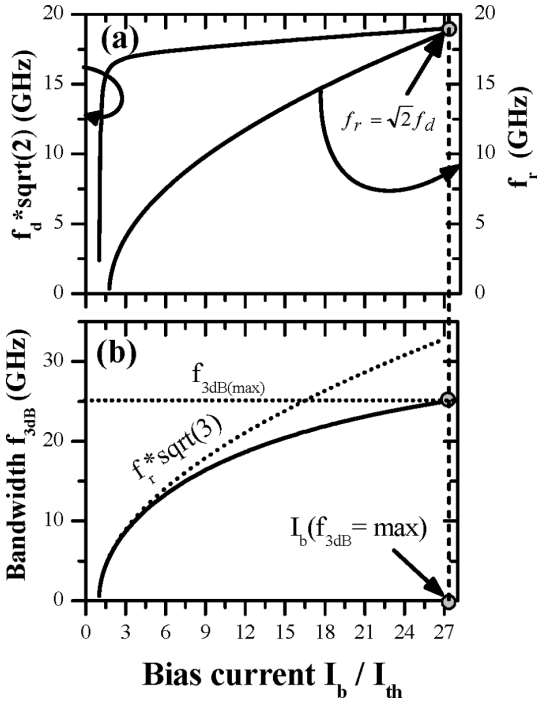

Figure 3. Influence of I_b on: (**a**) f_r and f_d and (**b**) $f_{3\mathrm{dB}}$. In (b) approximation of $f_{3\mathrm{dB}} \approx \sqrt{3} f_\mathrm{r}$ is plotted with the dashed line. The upper modulation frequency is 25 GHz corresponding to $I_\mathrm{b} = 27.1 I_\mathrm{th}$.

that Ω_r increases with I_b; it increases rapidly near-above threshold, $I_\mathrm{th} \leq I_\mathrm{b} \leq 1.3 I_\mathrm{th}$, and then increases sub-linearly when the laser is biased far-above threshold. This rapid increase of Ω_r over the near-threshold current range originates from the effective contribution of spontaneous emission to Γ_S in eq. (16), which in turn enhances Ω_r as given in eq. (23). By increasing I_b, the contribution of spontaneous emission to lasing characteristics diminishes [7]. The figure indicates also that Ω_r is greater than Γ_r, and their difference is apparently big when $I \gg I_\mathrm{th}$.

The corresponding variations of the damping frequency f_d and modulation bandwidth $f_{3\mathrm{dB}}$ with the bias current I_b are plotted in figures 3a and b, respectively. In figure 3a, f_d is multiplied by $\sqrt{2}$ and the relaxation frequency f_r is plotted on the right-hand axis in order to determine the value of I_b at which $f_\mathrm{r} = \sqrt{2} f_\mathrm{d}$. The figure shows that f_d increases rapidly with I_b for $I_\mathrm{th} \leq I_\mathrm{b} \leq 1.3 I_\mathrm{th}$, and further increase of I_b causes much smaller increase of f_d. This rapid increase of $f_\mathrm{d} = \Omega_\mathrm{r}^2/(4\pi\Gamma_\mathrm{r})$ near the threshold is manifested by the rapid increase of Ω_r with I_b, as given above, and the simultaneous linear increase of Γ_r shown in figure 2. Figure 3b shows that $f_{3\mathrm{dB}}$ increases with I_b. The increase is similar to that of f_r at the low range of I_b but is slower at the high range. The figure examines the validity of approximation (31), clarifying that this approximation is valid within the operation of conventional SL's, $I_\mathrm{th} \leq I_\mathrm{b} \leq 4 I_\mathrm{th}$. The accuracy of this approximation deteriorates with further increase of I_b. Numerical analysis of the data shows that the $f_{3\mathrm{dB}}$ vs. f_r curve is

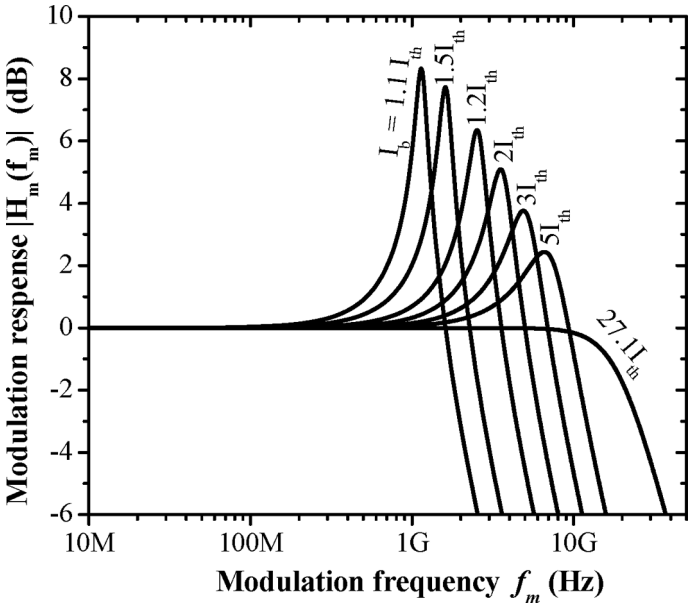

Figure 4. Variation of $|H_{\rm m}(f_{\rm m})|$ with bias current $I_{\rm b}$. The peak of the spectrum decreases with the increase of $I_{\rm b}$ and $|H_{\rm m}(f_{\rm m})|$ becomes flat when $I_{\rm b} = 27.1I_{\rm th}$.

fitted well by the third-order polynomial

$$f_{\rm 3dB} = \sqrt{3.46} f_{\rm r} - 1.8 \times 10^{-11} f_{\rm r}^2 - 4.71 \times 10^{-22} f_{\rm r}^3. \tag{37}$$

The ultimate upper modulation frequency $f_{\rm 3dB(max)}$ corresponds to the current $I_{\rm b}$ at which the curves of $f_{\rm r}$ and $\sqrt{2}f_{\rm d}$ intersect. Figure 3a indicates that this current is $I_{\rm b} = 27.1I_{\rm th}$, and figure 3b refers to $f_{\rm 3dB(max)} = 25$ GHz. This frequency is comparable to the values predicted by Bowers [26] and measured by Olshansky *et al* [13] and Stevens [17].

Variation of the response $|H_{\rm m}(f_{\rm m})|$ with the bias current $I_{\rm b}$ is shown in figure 4. $I_{\rm b}$ changes from $I_{\rm b} = 1.1I_{\rm th}$ to $27.1I_{\rm th}$ which corresponds to $f_{\rm 3dB(max)}$. The spectra exhibit the common feature that the low-frequency components are flat with $|H_{\rm m}(f_{\rm m})| = 1$. The figure shows that the peak value $|H_{\rm m}|_{\rm peak}$ decreases with the increase of $I_{\rm b}$, and the spectrum becomes flat when $I_{\rm b} = 27.1I_{\rm th}$. The response peak is then more visible at lower $I_{\rm b}$ due to the smaller values of $f_{\rm r}$ relative to $f_{\rm d}$. Except when $I_{\rm b} = 22I_{\rm th}$, the drop of $|H_{\rm m}|_{\rm peak}$ is seen to be associated with the shift of $f_{\rm m(peak)}$ towards higher frequencies $f_{\rm m}$. Numerical illustration of the dependences of $|H_{\rm m}|_{\rm peak}$ and $f_{\rm m(peak)}$ on $I_{\rm b}$ are given in figure 5. Figure 5a shows that $|H_{\rm m}|_{\rm peak}$ drops to much lower values with the increase of $I_{\rm b}$ until $I_{\rm b} \approx 3I_{\rm th}$, and then decreases slowly to $|H_{\rm m}|_{\rm peak} = 1$ when $I_{\rm b} = 27.1I_{\rm th}$. Figure 5b shows also that $f_{\rm m(peak)}$ has a parabolic dependence on I_b having a maximum value of 8.99 GHz when $I_{\rm b} = 13.7I_{\rm th}$. However, during the decreasing part of $f_{\rm m(peak)}$, the peak of the response is hardly pronounced in figure 4 because $|H_{\rm m}|_{\rm peak}$ is little higher than unity. The figure plots also the corresponding variation of $f_{\rm m(peak)}/f_{\rm r}$

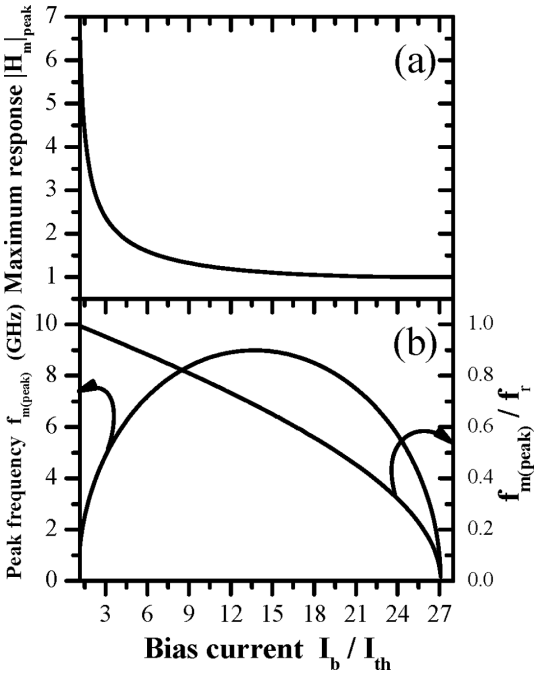

Figure 5. Influence of I_b on: (**a**) $|H_m|_{max}$ and (**b**) $f_{m(peak)}$ and frequency ratio $f_{m(peak)}/f_r$. $|H_m|_{peak}$ decreases with the increase of I_b. $f_{m(peak)}$ increases with I_b, peaking when $I_b = 13.7I_{th}$ and then decreases. When $I_b = 27.1I_{th}$, $|H_m|_{peak} = 1$ and $f_{m(peak)} \to 0$.

showing that this frequency ratio decreases with the increase of I_b and vanishes when $I_b = 27.1I_{th}$.

3.3 *Influence of gain suppression on modulation characteristics*

The gain suppression term BS_b increases with the photon number S_b, and consequently with I_b. Here, we illustrate the influence of gain suppression on the modulation characteristics by varying the nonlinear gain coefficient B relative to its value B_0 that corresponds to the parameters in table 1. Figures 6a and b plot the modulation response $|H_m(f_m)|$ as a function of B when $I_b = 3I_{th}$ and $20I_{th}$, respectively. Figure 6a shows that when $I_b = 3I_{th}$, gain suppression causes only a little decrease of the spectra around $f_{m(peak)}$. However, figure 6b indicates that this influence is significant when $I_b = 20I_{th}$ in the regime of high frequencies. The increase of gain suppression raises up the spectrum of $|H_m(f_m)|$ and shifts $f_{m(peak)}$ towards higher modulation frequencies.

The above effects can be understood by examining the influence of gain suppression on the damping rates Γ_S, Γ_N and Γ_r as well as the characteristics frequencies f_r, f_{3dB} and f_d. Figures 7a–d plot variations of these characteristics with I_b as functions of B. The figures show that over the range $I_{th} < I_b < 7I_{th}$, which covers

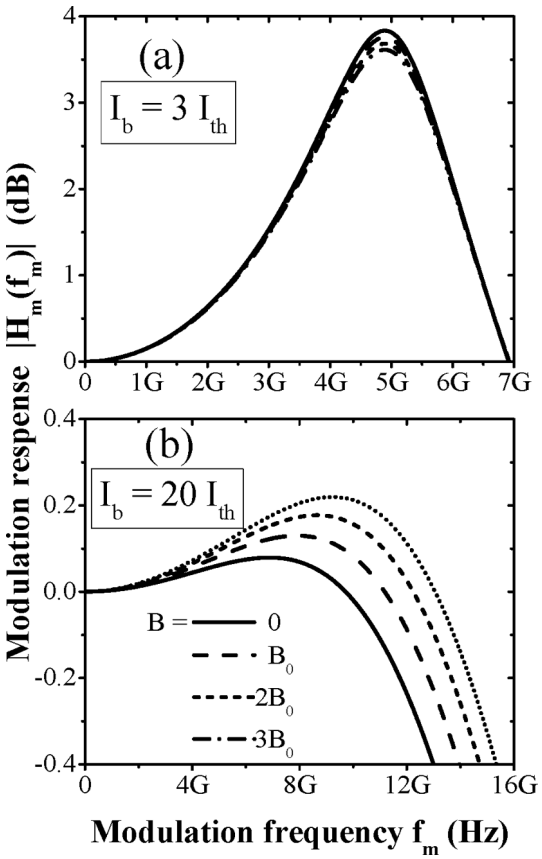

Figure 6. Modulation response $|H_{\rm m}(f_{\rm m})|$ as a function of B when: (**a**) $I_{\rm b} = 3I_{\rm th}$ and (**b**) $I_{\rm b} = 20I_{\rm th}$. Gain suppression significantly raises $|H_{\rm m}(f_{\rm m})|$ and increases $f_{\rm m(peak)}$ when $I_{\rm b} = 20I_{\rm th}$.

the operating range of conventional SL's, the influence of gain suppression is negligible except that $f_{\rm d}$ decreases little with the increase of B. This minor decrease of $f_{\rm d}$ explains the little decrease of $|H_{\rm m}(f_{\rm m})|$ in figure 6a. At higher $I_{\rm b}$, however, figures 7a and b show that gain suppression works to increase $f_{\rm r}$ and $f_{\rm 3dB}$ which agrees with the predictions of Agrawal [24]. Figure 7c shows that the increase of B increases the damping rate $\Gamma_{\rm S}$ of $S(t)$ as given in eq. (34). However, $\Gamma_{\rm N}$ decreases with B due to the decrease of $S_{\rm b}$ associated with the enhancement of gain suppression. The net result is a decrease of $\Gamma_{\rm r}$ and an increase of the damping frequency $f_{\rm d}$ as given in figure 7d. The figures show that the increase of $f_{\rm r}$ is relatively small when compared with the increase of $f_{\rm d}$. Therefore, the increase of gain suppression works to decrease the frequency ratio $f_{\rm r}/f_{\rm d}$, which then results in the increase of $|H_{\rm m}(f_{\rm m})|$ shown in figure 6b.

The influence of gain suppression on the ultimate upper modulation frequency $f_{\rm 3dB(max)}$ is also examined. Figure 8a plots variation of the ratio $f_{\rm r}/\sqrt{2}f_{\rm d}$ with the bandwidth $f_{\rm 3dB}$ as a function of B. These results correspond to the data shown in

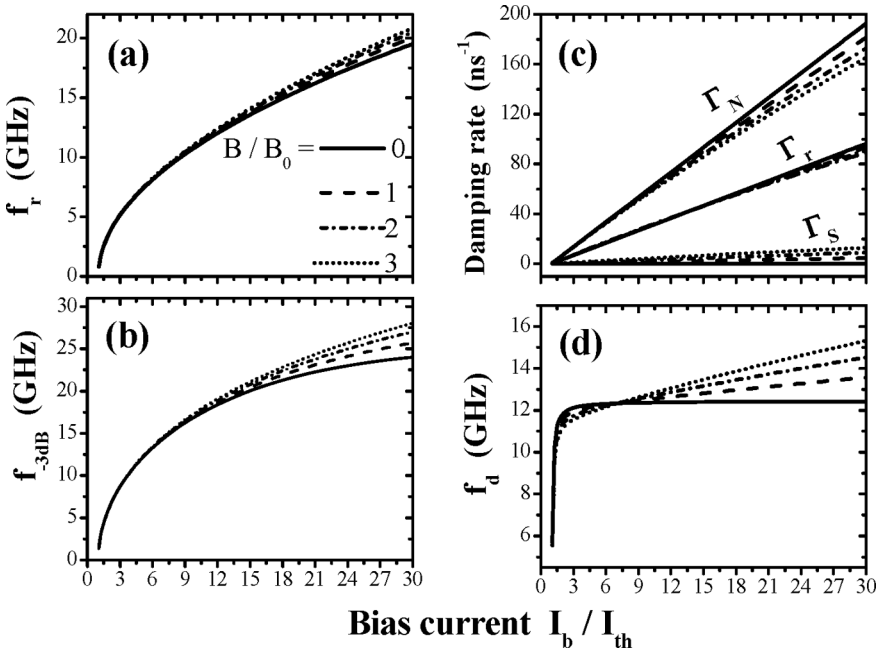

Figure 7. Influence of gain suppression on variations of: (**a**) $f_{\rm r}$, (**b**) $f_{\rm 3dB}$, (**c**) damping rates $\Gamma_{\rm S}$, $\Gamma_{\rm N}$ and $\Gamma_{\rm r}$ and (**c**) $f_{\rm d}$ with $I_{\rm b}$. Except for $\Gamma_{\rm N}$ and $\Gamma_{\rm r}$, the enhancement of gain suppression increases these modulation characteristics.

figure 7. A reference dashed line is plotted to indicate the condition of achieving flat modulation response $|H_{\rm m}(f_{\rm m})|$. The figure shows that $f_{\rm 3dB(max)}$, which is the frequency $f_{\rm 3dB}$ at which the curve intersects with the reference line, increases with the increase of B. That is, gain suppression is helpful to push $f_{\rm 3dB(max)}$ to higher values. As a numeric illustration, figure 8b plots the relation between the calculated values of $f_{\rm 3dB(max)}$ vs. B. Based on our knowledge, this quantitative description of the influence of gain suppression on $f_{\rm 3dB(max)}$ is newly introduced even though such influence has been extensively studied [7,11,16]. The shown increase of $f_{\rm 3dB(max)}$ with B is fitted well with the quadratic polynomial

$$f_{\rm 3dB(max)} = 23.1 + 1.78\frac{B}{B_0} + 0.1\left(\frac{B}{B_0}\right)^2 \ \text{(GHz)}. \tag{38}$$

This relationship enhances significance of the present quantitative dependence of $f_{\rm 3dB(max)}$ on gain suppression for 1.55-μm InGaAsP lasers. It provides to laser designers a guide to optimize the material and structural parameters that control gain suppression so as to maximize the modulation bandwidth. Conversely, it suggests a method to measure gain suppression, which is one of the most important physical parameters of 1.55-μm InGaAsP lasers, by measuring the modulation bandwidth.

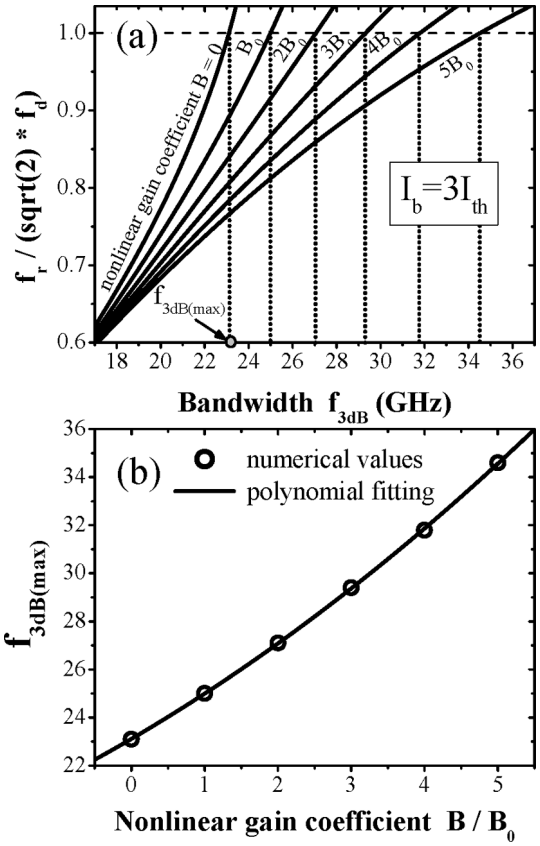

Figure 8. (**a**) Relation between $f_{\rm r}/\sqrt{2}f_{\rm d}$ and $f_{\rm 3dB}$ at different values of B and (**b**) variation of $f_{\rm 3dB(max)}$ with B. The cross-points of the curves in (a) with $f_{\rm r}/\sqrt{2}f_{\rm d} = 1$ determine $f_{\rm 3dB(max)}$. $f_{\rm 3dB(max)}$ increases with B according to eq. (38).

4. Conclusions

Theoretical characterization of the analog intensity modulation of SL's has been presented. The study was based on small-signal analysis and was focused onto 1.55-μm InGaAsP lasers. The obtained results showed that the modulation response peaks at a frequency less than or equal to the relaxation frequency depending on the bias current. Increasing the bias current is associated with decrease of the response peak; the response becomes flat when the bias current is 27.1 times the threshold current. The increase of the bias current is also associated with monotonical increase of the relaxation frequency, linear increase of the damping rate, and rapid increase of the bandwidth near the threshold followed by slower increase at higher bias levels. The maximum modulation bandwidth is 25 GHz. At bias levels well above the threshold, enhancing gain suppression results in increase of the modulation bandwidth and decrease of the damping rate, which gives rise

to increase of the maximum modulation frequency. Finally, we newly reported quantitative description of the dependence of the maximum modulation bandwidth on gain suppression.

References

[1] O Kjebon, R Schatz, S Lourdudoss, S Nilsson, B Stalnache and L Backbom, *Electron. Lett.* **33**, 488 (1997)
[2] G P Agrawal, *Fiber-optic communication systems* (J. Wiley & Sons Inc., New York, 2002)
[3] J Vanderwall and J Blackburn, *Opt. Lett.* **4**, 295 (1979)
[4] M Yamada and T Higashi, *IEEE J. Quantum Electron.* **27**, 380 (1991)
[5] D Bimberg, K Ketterer, H E Scholl and H P Vollmer, *Electron. Lett.* **20**, 343 (1984)
[6] O N Makeyev, Y A Zarkevitch and V I Smirnov, *Telecom. Radio Eng.* **45**, 41 (1990)
[7] K Petermann, *Laser diode modulation and noise* (Kluwer Academic, Dordrecht, 1988)
[8] C B Su and V Lanzisera, *Appl. Phys. Lett.* **45**, 1302 (1984)
[9] K Y Lau and A Yariv, *IEEE J. Quantum Electron.* **QE-21**, 121 (1985)
[10] R Olshansky, D M Fye, J Manning and C B Su, *Electron. Lett.* **21**, 721 (1985)
[11] G P Agrawal, *Appl. Phys. Lett.* **49**, 1013 (1986)
[12] D M Fye, R Olshansky and V Lanzisera, *Proc. 10th IEEE Semicond. Laser Conf.*, Kanazawa, Japan, 1986, p. 182
[13] R Olshansky, P Hill, V Lanzisera and W Powazinik, *Appl. Phys. Lett.* **50**, 653 (1987)
[14] E Henery, L Chusseau and J M Lourtioz, *IEEE J. Quantum Electron.* **26**, 633 (1990)
[15] F S Choa, Y H Lee, T L Koch, C A Burrus, B Tell, J L Jewell and R E Leibenguth, *IEEE Photonic Technol. Lett.* **3**, 697 (1991)
[16] G P Agrawal and N K Dutta, *Semiconductor lasers*, 2nd edition (Van Nostrand Reinhold, New York, 1993)
[17] R Stevens, *Modulation properties of vertical cavity light emitters*, Ph.D. thesis (Royal Institute of Technology, Sweden, 2001)
[18] M Ahmed, M Yamada and M Saito, *IEEE J. Quantum Electron.* **37**, 1600 (2001)
[19] H Haug, *Phys. Rev.* **184**, 338 (1969)
[20] M Ahmed, M Yamada and S W Z Mahmoud, *J. Appl. Phys.* **101**, 33119 (2007)
[21] M Ahmed and M Yamada, *J. Appl. Phys.* **84**, 3004 (1998)
[22] S Abdulrahmann, M Ahmed and M Yamada, *Opt. Rev.* **9**, 260 (2002)
[23] Y Suematsu and A R Adams, *Handbook of semiconductor lasers and photonic integrated circuits* (Chapman and Hall, London, 1994)
[24] G P Agrawal, *IEEE J. Quantum Electron.* **26**, 1901 (1990)
[25] C Y Wu, *Analysis of high-speed modulation of semiconductor lasers by electron heating*, Master Thesis (University of Toronto, Canada, 1995)
[26] J E Bowers, *Proc. 10th IEEE Semicond. Laser Conf.*, Kanazawa, Japan, 1986, p. 174